Chemical Engineering Science 313 (2025) 121749

Contents lists available at ScienceDirect

Chemical Engineering Science

journal homepage: www.elsevier.com/locate/ces

On the physical activation of biomass and urban waste chars for water treatment and CO_2 adsorption

Ledicia Pereira [a], Mónica Calero [a], Gabriel Blázquez [a], Sergio González-Egido [b], María González-Lucas [b], M. Ángeles Martín-Lara [a,*], Rafael R. Solís [a,*]

[a] *Valorization of Residues and Catalytic Processes Group, Department of Chemical Engineering, University of Granada, Avda. Fuentenueva s/n, 18071 Granada, Spain*

[b] *Environment and Bioproducts Group, Department of Life Sciences, University of Alcalá, Alcalá de Henares, 28871 Madrid, Spain*

A R T I C L E I N F O

Keywords:
Physical activation
Char
Water treatment
CO_2 adsorption
Waste recovery

A B S T R A C T

Different industrial chars, a subproduct result of the valorization of agroforestry, urban, and industrial residues by pyrolysis, were valorized using them as carbon precursors of activated carbons. The char derived from olive stones, acacia, pine residues, artificial cellulose, and spent recovered fuel (SRF, mixed urban waste, paper, and plastics) was submitted to physical activation with CO_2 (750 °C and 1 h). The activation led to materials with moderate surface area, i.e. 340–370 $m^2\ g^{-1}$, except for the SRF (136 $m^2\ g^{-1}$), and high micropores contribution (up to 83 % with olive stones). The chemical composition was characterized by elemental analysis, X-ray photoelectron spectroscopy, and temperature programmed desorption, which corroborated the presence of carbonyl and quinone groups. The activated samples were efficient in the adsorption of CO_2 from post-combustion gases (maximum uptake, 121 mg g^{-1} at 273 K and 100 kPa), strongly dependent on the micropores' contribution. The best sample displayed stable CO_2 uptake in dynamic cycles of adsorption–desorption. The activated samples were also evaluated as potential candidates for the adsorption of lead and caffeine in water decontamination.

1. Introduction

The ceaseless growth of population and the associated economic development to human beings embrace diverse drawbacks such as natural resources sought, the release of incessant polluting emissions, and the generation of wastes, among them, urban wastes that, without an alternative, are landfilled (Tejaswini et al., 2022). The deep concern of current societies about sustainable development and migration from carbon-based energy sources has been manifested internationally with diverse agreements signed under the United Nations negotiations.

The European Union is devoted to tackling more sustainable solid waste management based on a circular economy, minimizing landfilled residues (Gardiner and Hajek, 2020). In this sense, those residues that are not suitable for physical recycling are eligible for chemical valorization (Bhatt et al., 2021). Pyrolysis is an irreversible thermochemical transformation of carbon-enriched precursors at high temperatures (500–700 °C) under an oxygen-free atmosphere, promoting the lysis of larger chains, which triggers the formation of an oil, a syngas, and a solid residue named char (Qureshi et al., 2020). The operational conditions, mainly temperature, holding time, heating rate, and inert gas flow rate, define the yield and nature of each fraction. Although the valorization purpose is mainly focused on the maximization of oil and syngas phases, the applications for the char are still not well addressed, especially in those cases in which the residue comes from plastic or urban waste.

The chars obtained during thermochemical methods display poor textural properties (Apaydin-Varol and Pütün, 2012; Martín-Lara et al., 2021). For that reason, post-activation methods are required, in which physical and chemical activation can be stated (Heidarinejad et al., 2020). Although chemical activation has been stated as the most effective to boost textural properties, the impact of chemical substances, their hazard, and the further compulsory washing steps to remove the non-reacted chemicals compromise the cost and the environmental impact (Gao et al., 2020). Despite the fact that more responsible activation agents may alleviate some concerns (Sevilla and Fuertes, 2016), physical activation emerges as a plausible alternative. Physical activation relies on the thermochemical transformation at high temperatures, i.e. 700–900 °C, in the presence of reactive conditions, water, or CO_2 steam (Sakhiya et al., 2020). Between them, CO_2 has been widely used due to

---

* Corresponding authors.
E-mail addresses: marianml@ugr.es (M.Á. Martín-Lara), rafarsolis@ugr.es (R.R. Solís).

https://doi.org/10.1016/j.ces.2025.121749
Received 27 February 2025; Received in revised form 25 April 2025; Accepted 27 April 2025
Available online 29 April 2025

its higher ability to develop micropores, whereas H_2O steam triggers the formation of larger mesopores (González et al., 2009). For carbon capture and utilization applications, microporosity is largely preferred (Javed et al., 2021). During the activation process, volatile substances are released and occluded pores in the original char are opened and connected with others. Moreover, the gasification reactions of CO_2, which selectively react with the most reactive carbon, widen the microporosity of the surface (Liu et al., 2015). Multiple biomass-based biochars have been activated with CO_2 previously in the literature, including diverse residues of agroforestry activities (Thakur and Kumar, 2024).

Anthropogenic CO_2 emissions are one of the biggest challenges that humans face (Lee and Zhao, 2023). Carbon-based materials with a well-developed porosity can be potential candidates for carbon capture and storage. The advantages they display overcome the limitations of other materials; concretely, carbon materials benefit from low cost, simple synthesis, tunable design of porous and surface functional groups, fast kinetics, competitive selectivity towards certain adsorbates such as CO_2, etc. (Gunawardene et al., 2022). Besides, the treatment of water effluents for the adsorption of anthropogenic contaminants, either inorganic, such as metals (Mariana et al., 2021) or organic origin, like contaminants of emerging concern (Jeirani et al., 2017), is a mature and well-established technology in water treatment facilities, for both drinking water and sewage (Rashid et al., 2021).

This paper investigates the potential of physical activation for processed chars of different origins, including agroforestry residues (acacia and pine splinters), food industry (artificial cellulose used as packing agent and olive stones), and urban waste (recovered organic fractions including cardboard, paper, and plastics) for their valorization as activated carbons with adsorption properties. Although great efforts have been made to prepare activated carbon of boosted textural properties (Malini et al., 2023), little information is available regarding the activation of industrial chars released after the valorization of real biomass and industrial residues. Moreover, this work attempts to minimize the energy costs incurred by the activation process by selecting a milder activation temperature and a short activation time, also suggested by the lower activation time required by polymeric-based precursors (Pérez-Huertas et al., 2023). After activation with CO_2, the textural and chemical properties were evaluated, such as N_2 and CO_2 physisorption, immediate and elemental analysis, X-ray photoelectron spectroscopy, and temperature programmed desorption. The application of the activated chars was evaluated in two different scenarios, i.e. for CO_2 adsorption and storage in the gas phase, and water treatment for removing Pb as a representative inorganic pollutant, or caffeine, an organic pollutant of emerging concern.

2. Experimental section

2.1. Preparation of the activated chars

The chars used in this work were of industrial origin from a pyrolysis plant that obtains biofuel and syngas from urban, industrial, and agroforestry wastes. Five resulting chars obtained from the thermochemical valorization of very different wastes were considered, concretely olive stones (OS), acacia and pine splinters, artificial cellulose used in the food industry for packing purposes, and an industrial waste named as solid recovered fuel (SRF) made or urban wastes, paper, cardboards, and non-recyclable plastics. The chars, after the reception, were dried overnight at 120 °C. Next, they were submitted to physical activation with CO_2 at 750 °C. Firstly, N_2 (200 mL min^{-1}) was fed until reaching 750 °C (heating rate, 10 °C min^{-1}). Next, the gas was switched to CO_2 (200 mL min^{-1}) and the temperature was kept at 1 h and then naturally cooled. This temperature and the holding time were selected based on the ample information available in the literature that reports them as the average optimum for this process (Pérez-Huertas et al., 2023; Abuelnoor et al., 2021).

2.2. Characterization of the chars

The characterization of the textural properties was conducted by physisorption techniques. The N_2 adsorption and desorption isotherms were carried out by the standardized method at 77 K. A sync 200 physisorption device from 3P© instruments was used. The samples were outgassed overnight at 110 °C under a vacuum atmosphere. The total surface area was calculated using the BET method (S_{BET}). The total pore volume was determined from the N_2 consumption at a high relative pressure ($p/p_0 \sim 0.99$). The microporosity was quantified by the t-plot method, leading to the obtention of the micropore surface (S_{MP}) and volume (V_{MP}). The micropore size distribution was calculated from the CO_2 isotherms carried out at 273 K. The Horvath–Kawazoe (HK) method was applied for the determination of the pore size distribution (Dombrowski et al., 2001; Gauden et al., 2004).

The carbon content was determined in a first approach by proximate analysis. The relative proportions of moisture, volatiles, fixed carbon, and ash were quantified by thermogravimetry analysis under an inert atmosphere. A PerkinElmer STA 6000 thermobalance was used, raising the temperature and the sample from room temperature to 110 °C (40 °C min^{-1}) under 20 mL min^{-1} of N_2, and holding for 10 min to calculate the moisture. Then, the temperature was raised to 875 °C (40 °C min^{-1}) to quantify the volatile contribution. Next, the N_2 flow was exchanged by O_2 (20 mL min^{-1}) to promote the combustion of the fixed carbon. Finally, the sample was cooled, leaving for the obtention of the ashes. Elemental analysis was used to determine the content of C, H, N, and S in a Thermo Scientific Flash 2000 device. The contribution of O was tentatively estimated by difference after removing the ash contribution. The chemical composition of the surface was studied by X-ray Photoelectron Spectroscopy (XPS). The analysis was conducted in a Kratos AXIS Ultra-DLD device irradiated with an X-ray source from Al Kα. The spectra were corrected to 284.6 eV in the C_{1s} peak with Shirley background correction. The spectra were processed with the software XPSpeak 4.1. The analysis of the surface was completed with Chemisorption analysis, and conduction Thermal Programmed Desorption (TPD) with NH_3 to compare the acidity of the materials and the surface functional groups. The device used was an AMI-300Lite chemisorption station from Altamira Instruments® coupled to Thermal Conductivity Detection (TCD). About 100 mg of the sample was placed in a quartz ‘U’ shape reactor and submitted. After drying at 110 °C with He (25 mL min^{-1}), the adsorption step was carried out with NH_3 (10 %NH_3 in He, 25 mL min^{-1}) under 100 °C for 1 h. Finally, a temperature program from 100 °C to 1000 °C was applied under He (25 mL min^{-1}), and the TCD signal was recorded.

The pH at the point of zero charge (pH_{pzc}) was estimated by the standard acid-base titration procedure (Rajah et al., 2019). Solutions containing 50 mL of NaCl 0.1 M were prepared and the pH adjusted to an initial desired value, between 2 and 10. Then, the solid material was incorporated at a dose of 2 g L^{-1}, and the pH after reaching equilibrium was measured. The pH_{pzc} was calculated from the bisector of the initial and final pH values.

2.3. Carbon dioxide adsorption experiments

The CO_2 adsorption experiments were carried out in two different setups. Firstly, characterization tests of the CO_2 adsorption process were conducted under static conditions in a sync 200 physisorption device from 3P© instruments. The CO_2 isotherms were obtained at two different temperatures, i.e. 273 and 298 K. These two isotherms were used to calculate the CO_2 isosteric adsorption heat (ΔH_{ads}) as a function of the CO_2 uptake coverage. Hence, the equation of Clausius–Clapeyron was considered in combination with the Freundlich isotherms (Pereira et al., 2024; Ligero et al., 2024; He et al., 2021).

The CO_2:N_2 selectivity at 298 K was calculated considering the Ideal Adsorbed Solution Theory (IAST) (Bell et al., 2021). An isotherm of N_2 at 298 K was obtained. Both CO_2 and N_2 isotherms were fitted to the

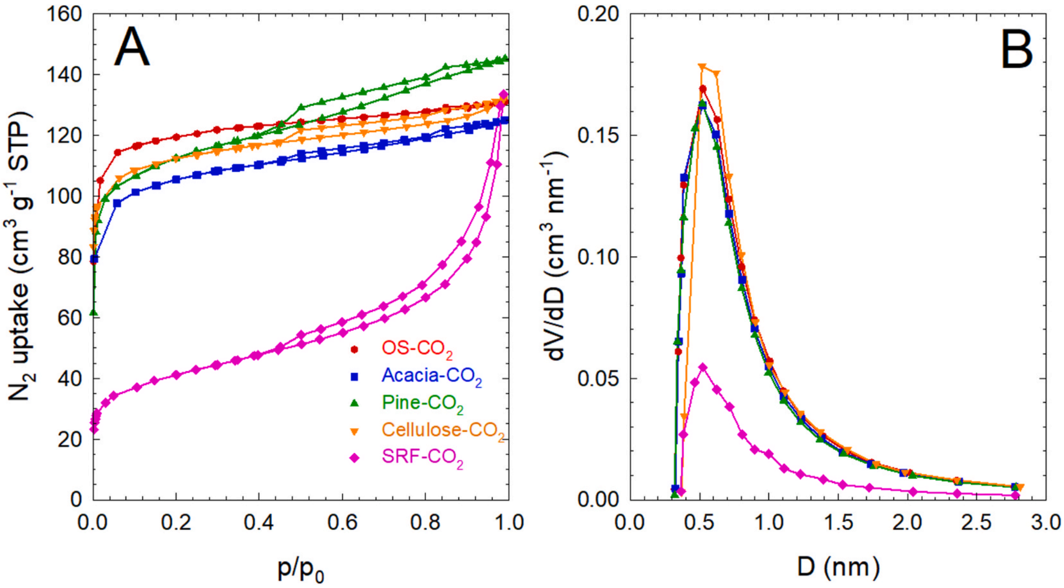

Fig. 1. Textural characterization by physisorption analysis of the CO$_2$-activated chars with N$_2$ adsorption–desorption isotherms at 77 K (A) and the micropore size distribution obtained from CO$_2$ adsorption isotherm at 273 K with the HK method (B).

Freundlich model to predict the volume gas uptake with pressure, and the selectivity as a function of the pressure for a typical post-combustion mixture of 15:85 CO$_2$:N$_2$ was calculated as follows (Liao et al., 2015; Solís et al., 2023):

$$S = \frac{\frac{V_{CO_2}}{P_{CO_2}}}{\frac{V_{N_2}}{P_{N_2}}} = \frac{V_{CO_2}}{V_{N_2}}\frac{85}{15} \tag{1}$$

where V$_i$ means the gas uptake (STP cm^3 g^{-1}) at a certain pressure and p$_i$ is the partial pressure of the i component in the mixture.

Dynamic tests of CO$_2$ adsorption were conducted in a lab-made jacketed Pyrex glass column (10 cm high and 1 cm internal diameter). The bed temperature was controlled by pumping refrigerant through the annular space of the column at 25 °C. The column was loaded with 1 g of activated carbon, which was retained with the aid of inert glass balls. Two mass flow controllers produced a gas mixture of CO$_2$ and N$_2$ (100 mL min^{-1}) at different proportions, the CO$_2$ concentration ranging from 10-40 %. A continuous Non-Dispersive InfraRed (NDIR) detector (NDIR Edinburgh Instruments Ltd.) was placed at the column exit to monitor the CO$_2$ concentration leaving the column. The adsorbed CO$_2$ was calculated from the area below the removed CO$_2$, from the begining of the test until reaching the saturation time (95 % of the fed CO$_2$):

$$q_{CO_2} = \frac{\upsilon\, C_{inlet}}{m_{sample}} \int_0^t \left(1 - \frac{C_t}{C_{inlet}}\right) dt \tag{2}$$

where υ (L s^{-1}) is the volumetric flow rate, C$_{inlet}$ (mol L^{-1}) stands for the inlet CO$_2$ concentration, and m$_{sample}$ (g) means the loaded mass of activated carbon in the column. For the desorption curve, the inlet gas was changed to 100 % N$_2$, flow rate 100 mL min^{-1}, until no release of CO$_2$ in the outlet. Before each experiment, a baseline check was conducted and zeroed.

Table 1
Characterization of the textural properties by N$_2$ physisorption at 77 K.

Sample	S$_{BET}$ (m^2 g^{-1})	S$_{MP}$ (m^2 g^{-1})	V$_T$ (cm^3 g^{-1})	V$_{MP}$ (cm^3 g^{-1})	V$_{UMP}$ (cm^3 g^{-1})	V$_{MP}$/V$_T$ (%)
OS-CO$_2$	363.2	328.1	0.203	0.170	0.121	83.7
Acacia-CO$_2$	341.8	291.2	0.193	0.142	0.123	73.6
Pine-CO$_2$	367.9	286.7	0.225	0.139	0.095	60.4
Cellulose-CO$_2$	359.7	341.6	0.204	0.155	0.137	76.0
SRF-CO$_2$	136.1	61.7	0.207	0.039	0.031	18.8

S$_{BET}$: total surface area by BET method; S$_{MP}$, micropore surface; V$_T$, total pore volume from p/p$_0$ ~ 0.99 uptake; V$_{MP}$, micropore volume; V$_{UMP}$, ultramicropore volume (<0.7 nm).

2.4. *Adsorption tests in the aqueous phase*

The adsorption capacity of the physically activated carbon was assessed by the obtention of the adsorption isotherms, conducted in 100 mL flasks under batch mode at 25 °C. The adsorbent was added at a dose of 2 g L^{-1} in 50 mL solutions of different concentrations of Pb^{2+} (10–320 mg L^{-1}) or caffeine (10–640 mg L^{-1}). The slurry was kept under vigorous stirring until it reached equilibrium. Samples before and after adsorption were withdrawn for analysis and filtered with commercial syringe filters (Millipore, Millex-GV PVDF, 0.45 µm). The concentration of Pb^{2+} was quantified by Flame Atomic Absorbance spectrometry in a PinAAcle 500 spectrometer from PerkinElmer®. The concentration of caffeine was analyzed by High-Pressure Liquid Chromatography (HPLC), coupled with molecular absorbance spectrophotometric detection. The chromatograph used was an Alliance e2695 apparatus from Waters™ in which a 2998 photodiode array UV–visible module was connected. The analyte separation was carried out in a Zorbax Bonus-RP column (4.6 × 150 mm, 5 µm). The mobile phase, pumped at a rate of 1 mL min^{-1}, was a mixture of acetonitrile (A) and acidified water with 0.1 % (vol.) of trifluoroacetic acid (B) with a constant A: B ratio of 15:85. The absorbance at 275 nm was selected for the quantification. The concentration was measured in each flask before and after adding the adsorbent to determine the adsorbate uptake, and the resulting isotherms were successfully fitted to the three-parameter Sips's model (Sips, 1948).

The dynamic behavior was tested in a fixed-bed column. The set-up consisted of a jacketed column (11 cm height, 1.5 cm internal diameter), thermostated at 25 °C. The column was loaded with 0.5 g of activated carbon, sieved at 355–500 µm to avoid bed compaction, and retained with glass spheres and wool. The column was operated in continuous pumping of Pb^{2+} (20 mg L^{-1}) or caffeine (20 mg L^{-1}) at an average flow rate of 2 mL min^{-1}. For the desorption experiments, a solution consisting of aqueous HCl 1 M in the case of desorption of Pb^{2+} and methanol in the

Table 2
Proximate and elemental analysis of the chars physically activated with CO_2.

Sample	Proximate analysis (%)				Elemental analysis (%)		
	Moisture	Volatile	Fixed carbon	Ash	C	H	O*
OS-CO_2	3.6	8.4	85.2	2.8	55.1	1.1	43.8
Acacia-CO_2	6.9	7.0	85.7	0.4	88.4	1.2	10.4
Pine-CO_2	4.6	6.2	85.5	3.7	84.4	1.2	14.4
Cellulose-CO_2	4.1	6.2	87.7	2.0	71.0	1.2	27.8
SRF-CO_2	2.9	5.9	68.2	23.0	60.0	0.8	36.7

* After subtraction of the ashes. N content was negligible in all the samples.

case of caffeine was fed at the same flow rate.

3. Results and discussion

3.1. Characterization of the activated materials

The main goal of the activation process relies on the improvement of the textural properties, enlarging the porosity of the carbonaceous char. For this purpose, N_2 adsorption–desorption isotherms were carried out, as illustrated in Fig. 1. The original chars displayed negligible surface area, i.e. values below 1 $m^2\ g^{-1}$ (OS, pine, and cellulose), or very low, i.e. inferior to 25 $m^2\ g^{-1}$ (acacia and SRF). The activation with CO_2 raised the porosity of the samples, see Table 1 with values in the range of 340–370 $m^2\ g^{-1}$, except for the SRF-CO_2, 136 $m^2\ g^{-1}$, probably due to the recalcitrant nature of this residue for the reaction with CO_2. The surface areas are less impressive than the reported chemical activation with alkali (Pereira et al., 2024; Lim et al., 2023) or carbonates (Solís et al., 2024). Nonetheless, the values obtained are at the same level as other char feedstocks (Sakhiya et al., 2020). The activation with CO_2 of char obtained in the pyrolysis with N_2 of pine sawdust has been reported to reach 336 $m^2\ g^{-1}$ (activated at 800 °C, 1.5 h) (Patel et al., 2023), very close to the 367 $m^2\ g^{-1}$ of this work. For olive stone, the activation of a char with an initial surface higher than the one reported in this study, i.e. 209 $m^2\ g^{-1}$, which led to a rise after CO_2 activation (850 °C, 1 h) to 572 $m^2\ g^{-1}$ (Román et al., 2008), which means an increase of 363 $m^2\ g^{-1}$ during the activation, the same as the one obtained in this work. In other work, a hydrochar derived from olive stones generated during hydrothermal treatment was also activated under CO_2 steam (750 °C, 1 h), leaving a porous material of 449 $m^2\ g^{-1}$ (Bourafa et al., 2023). The CO_2 activation of acacia residues has been reported to have very similar values, 395 $m^2\ g^{-1}$ (Danish et al., 2013). Residues of cellulose, submitted to pyrolysis and after a second step of CO_2 activation (600 °C, 1 h) were reported to reach 434 $m^2\ g^{-1}$, slightly higher than the 359 $m^2\ g^{-1}$ obtained in this work. SRF is a complex mixture based on spent residues fuel with an important contribution of plastic waste, whose activation may be like plastic char that, after activation, has exhibited an area of around 100 $m^2\ g^{-1}$ (Ligero et al., 2023).

According to the IUPAC's classification (Sing et al., 1985), the isotherms of the activated samples, except for SRF-CO_2, are described as Type I with H4 hysteresis loop in Acacia-CO_2 and Pine-CO_2, as reported for other biomass precursors (Serafin et al., 2017). This shape embraces the strong presence of narrow micropores, i.e. <1 nm (Thommes et al., 2015). After filling the micropores at low relative pressures, a plateau is reached. In contrast, the sample SRF-CO_2 defines a Type II isotherm with the definition of a knee, characteristic of mesoporous materials (Bläker et al., 2019). The determination of the micropore contribution by the t-plot method corroborates these facts in the values obtained for the microporous surface and pore volume and their contributions. As a matter of fact, the microporosity understood as the ratio in terms of pore volume, was high, over 60 %, in all the samples except for SRF-CO_2. Remarkably high was the ratio defined by the sample OS-CO_2, i.e. 83 %. Instead, the SRF-CO_2 displayed mostly mesoporosity, accounting for

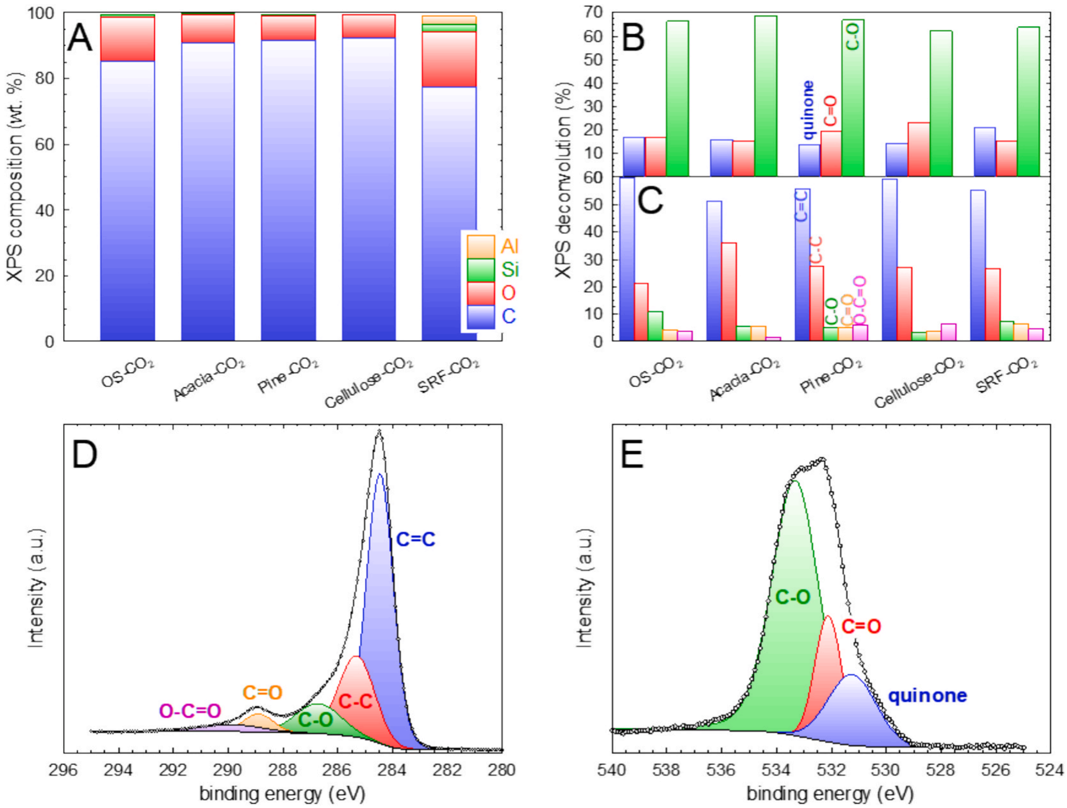

Fig. 2. Characterization of the activated chars by XPS. Surface composition (A), deconvoluted contributions obtained in C_{1s} (B) and O_{1s} (C) regions, and example of deconvolution of the C_{1s} (D) and O_{1s} (E) regions of OS-CO_2.

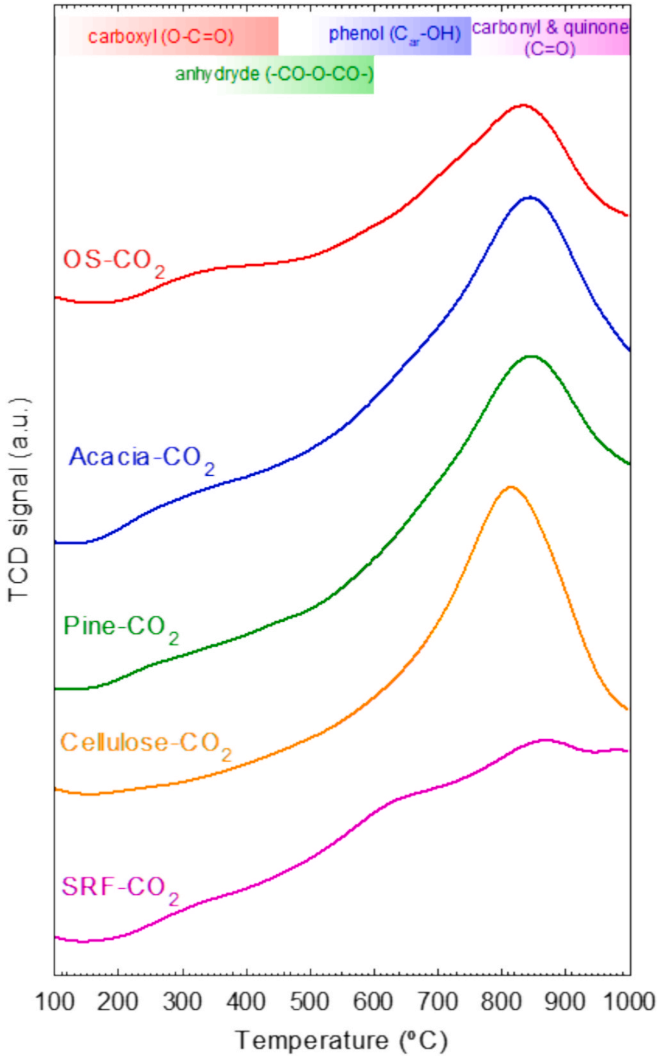

Fig. 3. Chemisorption characterization with TPD of the chars activated with CO_2.

only 15 % of micropores. Regarding the hysteresis loop in the desorption step, it can be observed that the most porous samples did not define a clear loop. Only the sample pine-CO_2 timidly described an H4 loop, which is consistent with the lowest microporosity, 60 %, the group among these samples. The SRF-CO_2 performed a very different behavior, with an H3 loop. Fig. 1 also illustrates the pore size distribution, confirming the presence of micropores whose average size is centered at approximately 0.4–0.6 nm. It is also deduced that the sample SRF-CO_2, the most mesoporous, accounted for a much smaller presence than the rest.

The composition and carbon content were analyzed by proximate and elemental analysis and XPS techniques, respectively. The results achieved are summarized in Table 2 and Fig. 2. In general, when comparing the samples, it is evident that the activated carbon obtained from acacia, pine, and cellulose displayed the highest carbon content, as both the fixed carbon and the C percentage from elemental analysis corroborate. The lignocellulosic origin of their char provides them with an elevated carbon content (Pereira et al., 2024). The olive stone displayed a particular behavior. Although fixed carbon suggests a high carbon content, the elemental analysis verified 55 %, which is consistent with the origin of the olive stones (Rajah et al., 2019), which usually displays around 50 %. After the activation reaction, some active superficial carbon reacts with the $CO_{2,}$ triggering the formation of CO (Di Blasi, 2009), leaving a similar composition in terms of the bulk (Pereira et al., 2024; García Martín et al., 2020). The sample SRF is the result of a char obtained from solid recovered fuel, mainly composed of organic waste, paper, and cardboard, mixed with non-recyclable plastic, which makes it a solid poorly enriched with carbon (Pereira et al., 2024). This fact explains why the content after activation was lower than the other samples, whose origin was lignocellulosic.

The surface chemical composition was evaluated by the XPS technique due to its relevance for practical applications such as adsorption. Fig. 2 depicts the surface composition obtained by XPS, the contribution to the deconvoluted peaks of C_{1s} and O_{1s} for all the samples, and the high resolution spectra of C_{1s} and O_{1s} regions of one of the samples, i.e. OS-CO_2. The surface composition, although different from the bulk values obtained by elemental analysis, conserves the same relative behavior among the samples. The activation of acacia, pine, and cellulose led to over 90 % of surface C. The O content was the lowest in these three samples, 7.0–8.5 %. The difference between surface and bulk was more remarkable in the cases of OS-CO_2 (85 %) and SRF-CO_2 (77 %). Moreover, these two samples performed the highest O content on their surface, i.e. 13.4 % in OS-CO_2 and 16.7 % in SRF-CO_2. This latter material corroborated the presence of Si and Al at roughly 2 %, evidencing the complexity of the waste used for the preparation. The high-resolution spectrum of C_{1s} was explained based on the contributions of sp^2 C═C (284.4 eV), sp^3 C–C (285.3 eV), C–O (286.5 eV), C═O (288.5 eV), and O-C═O (290.0 eV) (Ramírez-Valencia et al., 2023). The O_{1s} region was deconvoluted in quinone (531.0 eV), C═O (532.0 eV), and C–O (533.0 eV) (Burg et al., 2002). According to the deconvolutions, the two most oxygenated samples, i.e. OS–CO_2 and SRF-CO_2, displayed the highest content of C-O bonds to the detriment of sp^3 C–C. The activated chars prepared from acacia, pine, and cellulose were the most enriched in carboxylic acids. From the O_{1s} region, it was evident that the predominant oxygenated group was the C–O. The SRF-CO_2 displayed the highest contribution of quinones, and the cellulose-CO_2 outstanding the high content of C═O.

The surface was further characterized by chemisorption analysis with ammonia TPD. The desorption TPD profiles are illustrated in Fig. 3. The acidity and the nature of the oxygenated groups were further corroborated by chemisorption analysis. For the interpretation of the TPD profiles, the temperature at which different bands appeared were classified as follows: carboxyl below 450 °C, anhydride at 350–600 °C, phenol at 500–750 °C, and carbonyl-quinones at 750–1000 °C (Shafeeyan et al., 2010; Rocha et al., 2023; Herold et al., 2022). According to the TPD areas below the curves, the acidity followed the order of Cellulose-CO_2 > Acacia-CO_2 > Pine-CO_2 > OS-CO_2 ≫ SRF-CO_2. As stated by the deconvolution of O_{1s} of XPS, the desorption profiles proved a major contribution of carbonyl and quinones in all the samples, in the order described previously. Only the samples OS-CO_2 and Acacia-CO_2 defined a timid shoulder in the region of carboxylic acids. The sample SRF-CO_2 did not perform any substantial acidity character and the TPD profile barely suggests a minor presence of carbonyl/quinones and phenolic groups.

3.2. *Carbon dioxide adsorption*

The adsorption capability of the physically activated chars was analyzed by conducting static physisorption isotherms up to 100 kPa with CO_2 at two temperatures, 273 and 298 K. The results are depicted in Fig. 4A. The CO_2 isotherms, see Fig. 4A, depict the typical Freundlich isotherm due to the reversibility, non-ideality, and plausible multilayer adsorption of CO_2 onto activated carbons. The values at 273 K and ambient pressure followed the order OS-CO_2 (121 mg g^{-1}) > Acacia-CO_2 (115 mg g^{-1}) = Cellulose-CO_2 (115 mg g^{-1}) ~ Pine-CO_2 (112 mg g^{-1}) and ≫ SRF-CO_2 (36 mg g^{-1}). The dependency of the CO_2 uptake and the micropore volume is illustrated in Fig. 4B, leading to a linear tendency that can presumably be assumed as proof of the importance of micropore development. The textural properties play an essential role during the adsorption of non-polar molecules (Rodriguez-Reinoso et al., 1992),

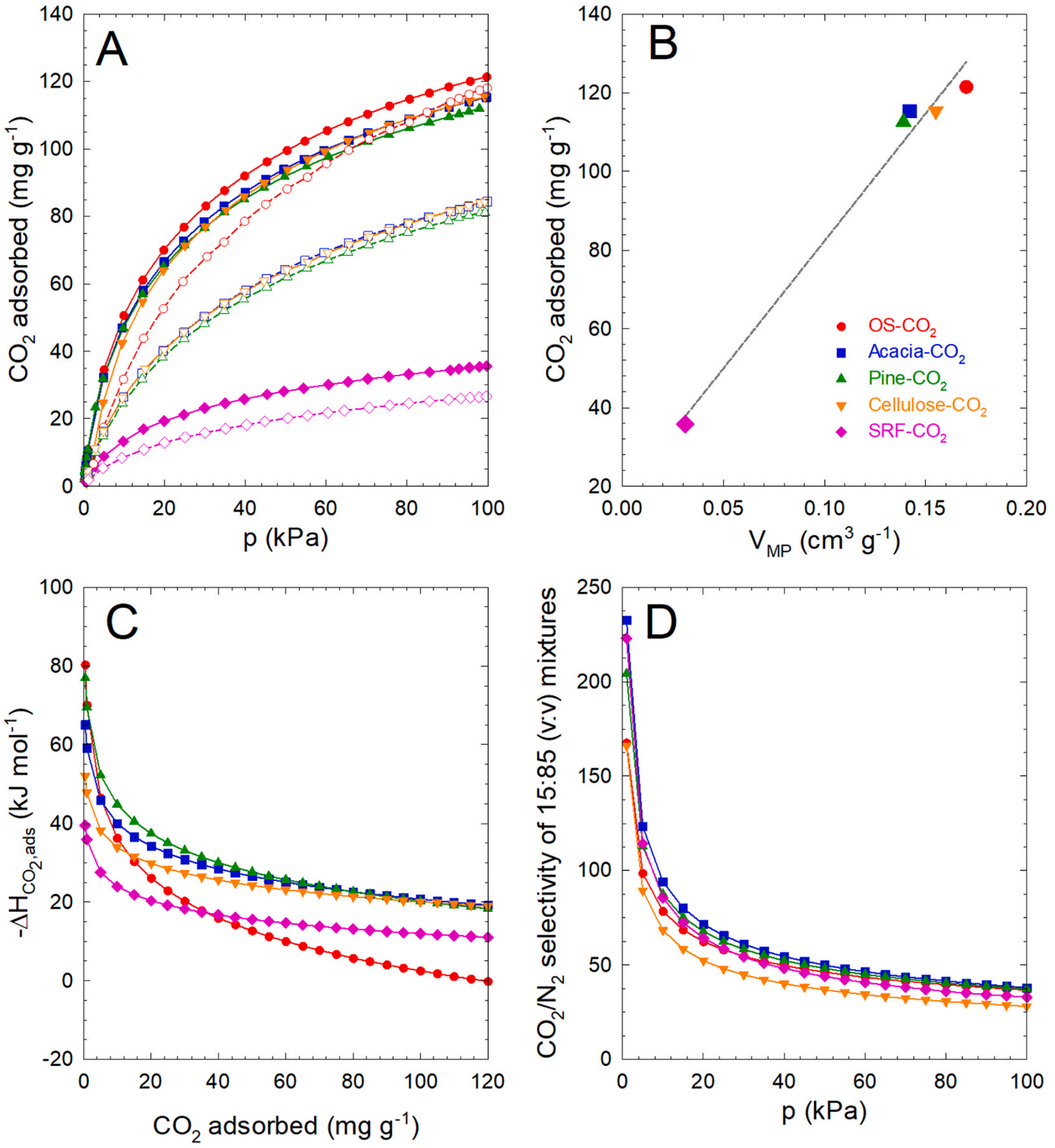

Fig. 4. Adsorption of CO_2 of the activated chars. CO_2 isotherms at 273 K (filled symbols) and 298 K (empty symbols) (A), the relationship of the CO_2 uptake at 273 K and the micropore volume (B), the isosteric adsorption heat (C) and the selectivity of a post-combustion CO_2/N_2 mixture of 15:85 (v/v) (D).

such as CO_2, mainly characterized by physical interactions, driven by the filling of the micropores. The presence of micropores is of paramount importance for capture at low pressures (Shen, 2022), concretely ultramicropores, in the range of 0.5–0.9 nm (Mochizuki et al., 2024), which serve as the optimum active sites for effective interaction. Furthermore, the existence of an adequate functional group results in enhanced selectivity of CO_2 compared with other gases. The polarity of the carbon surface significantly affects CO_2 adsorption, such as hydroxyl and carboxyl groups (He et al., 2023). The determination of the binding energy of physisorption from the interaction of the CO_2 molecule and edge oxygenated groups has been stated to have greater interaction for carboxyl and hydroxyl groups, being quinone and carbonyl, less polar, practically the same as pristine carbon (Liu et al., 2018). Although all the precursors except SRF led to very similar textural properties, the OS-CO_2 led to slightly higher performance in CO_2 adsorption, which may be ascribed to the lower content of carbonyl/quinone if compared to carboxyl, as deduced from the chemisorption analysis.

The adsorbed CO_2 at 273 K and ambient pressure is high considering the micropore volume. The adsorbed CO_2 per unit of micropore volume ranged from 715-812 mg cm^{-3}. These values are high compared to those reported in the literature. In previous work on these materials activated with KOH, the values were 300–500 mg cm^{-3} (Pereira et al., 2024). For olive stone activated with CO_2, this ratio has been reported as 466 mg cm^{-3} (activation at 1000 °C, 30 min), lower than the material of this study (Puig-Gamero et al., 2021). A value of 410 mg cm^{-3} has been published for olive stones activated for 6 h at 800 °C (González et al., 2013). For instance, pine sawdust submitted to pyrolysis and CO_2 activation (800 °C, 1.5 h) led to 663 mg cm^{-3} (Patel et al., 2023). In the case of cellulose, a value of 552 mg cm^{-3} has been reported (activation 800 °C, 1 h) (Heo and Park, 2015). However, other materials have reported similar or incredibly higher values, for instance, activated mesoporous biocarbon (1355 mg cm^{-3}) (Singh et al., 2017), gelatin: starch mixtures activated with KOH (646 mg cm^{-3}) (Alabadi et al., 2015).

The isotherms were obtained at two different temperatures, i.e. 273 and 298 K, registering a decay of CO_2 uptake, as the result of the exothermicity of the process, more important in the samples prepared from acacia, pine, and cellulose. This behavior evidences not only the exothermicity of the process but also a plausible influence of the oxygenated groups in the thermodynamics of the process, as the samples OS-CO_2 and SRF-CO_2 displayed higher surface oxygen, and their CO_2

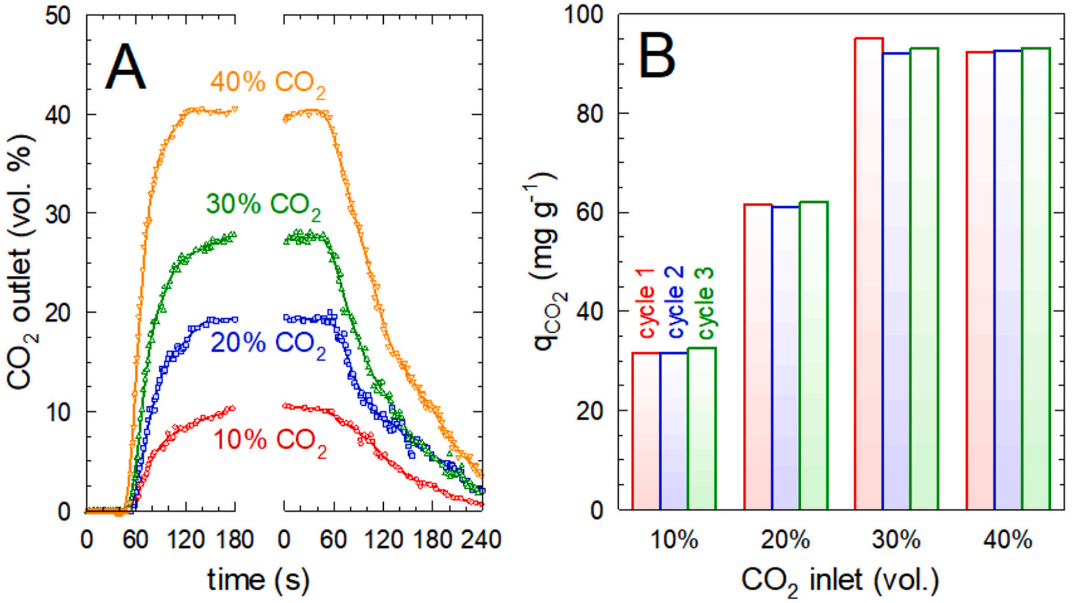

Fig. 5. CO$_2$ adsorption and desorption breakthrough curves at different inlet concentrations (10–40%) with OS-CO$_2$. An example of a cycle of adsorption and desorption breakthrough curve (A) and the CO$_2$ saturation capacity in three consecutive cycles (B).

uptakes were less affected by the decrease of the temperature, i.e. less exothermic. The CO$_2$ isosteric adsorption heat versus the CO$_2$ coverage is illustrated in Fig. 4C. An asymptotic trend with the CO$_2$ uptake degree was observed by all the materials, as a consequence of the heterogeneity of the surface, in which the most preferred active sites are covered at low pressures. The isosteric adsorption heat is higher in the micropore range, i.e. at low pressures (Fan et al., 2016). Once the micropores are filled, the adsorption heat reaches a plateau. The heat tends to ~ 20 kJ mol^{-1} for acacia-CO$_2$, pine-CO$_2$, and cellulose-CO$_2$, whereas SRF-CO$_2$ led to ~ 10 kJ kmol$^{-1,}$ and OS-CO$_2$ led to a null value. These values prove the higher interaction of the three former materials, although labeled as a physisorption interaction due to the low values (Saleh, 2022). The results are within the expected range in the literature for other biochars physically activated with CO$_2$ (González et al., 2013; Sarwar et al., 2021).

Finally, the characterization behavior in static experiments was completed with the estimation of the selectivity at 25 °C by the IAST method for a post-combustion mixture of 15:85 proportion of CO$_2$:N$_2$. As depicted in Fig. 4D, all the samples performed quite similar trends, a logarithmic curve whose asymptote tends to selectivity value of 28 (Cellulose-CO$_2$)-38 (Acacia-CO$_2$). This decrease is linked to the preference of micropores, concretely ranging 0.7–1.5 nm, for the adsorption of CO$_2$ (Fan et al., 2016). These values were higher than those reported previously in the literature for pine sawdust at similar conditions, either activated with CO$_2$ or KOH, 17 and 12, respectively (Patel et al., 2023).

Based on the higher performance of the sample OS-CO$_2$, further analysis under dynamic adsorption tests of CO$_2$-N$_2$ mixtures was performed. The influence of the inlet CO$_2$ concentration was evaluated in the range of 10–40 % during three consecutive cycles, as depicted in Fig. 5. Regardless of the inlet CO$_2$ concentration, the breakthrough time was barely affected by the inlet CO$_2$ concentration, around 60 s. The CO$_2$ uptake during the adsorption cycle increased as the inlet concentration was raised, i.e. the average values during the three cycles were 31.9 ± 0.5 mg g^{-1} (10 %), 61.5 ± 0.4 mg g^{-1} (20 %), 93.3 ± 1.5 mg g^{-1} (30 %), and 92.6 ± 0.4 mg g^{-1} (40 %). This effect can be ascribed to the increased probability of interaction between the adsorbate and the surface of the adsorbent. Moreover, the established CO$_2$ gradient is larger when the inlet concentration is raised; therefore, the mass resistance opposed to the transfer is diminished (Tan et al., 2014; Hook, 1997; Ligero et al., 2023). These values were inferior to those obtained in the static test (121 mg g^{-1}). These differences may be attributed to diffusion limitations during the gas flow in the bed, for which the presence of mesopores may help as a first shuttle to the micropores where CO$_2$ is retained (Manyà et al., 2020). Regarding the desorption step, a slower process was achieved, i.e. 240 s for being completely desorbed in all the cases, which benefits the stability of the material for sequential adsorption–desorption cycles. The material displayed great stability during the reutilization in sequential adsorption–desorption cycles at the four inlet CO$_2$ concentrations tested, as visible in Fig. 5B at different inlet CO$_2$ concentrations. Very few variations during the cycles were detected, being inferior to 2 % in all cases, which provides evidence of the physisorption nature of the process and the lack of adsorption effectiveness.

3.3. *Adsorption of pollutants in water*

The performance of the CO$_2$-physical activated chars was evaluated for water treatment applications. Two different pollutants were selected based on their ubiquitous presence either in industrial or urban wastewater, i.e. lead (Madhav et al., 2020) and contaminants of emerging concern such as caffeine (Buerge et al., 2003; Li et al., 2020; Korekar et al., 2019). Firstly, equilibria batch tests were conducted with all the activated materials, leading to the adsorption isotherms of Pb and caffeine depicted in Fig. 6.

The adsorption of Pb was moderate if compared to other materials, with maximum adsorption uptakes, in the range of study, following the order SRF-CO$_2$ (25.5 mg g^{-1}) > Cellulose-CO$_2$ (18.5 mg g^{-1}) > Acacia-CO$_2$ (15.5 mg g^{-1}) > OS-CO$_2$ (13.5 mg g$^{-1)}$ > Pine-CO$_2$ (11.0 mg g^{-1}). The isotherms were successfully fitted to the Sips model, see Fig. 6A and Table 3, with no definition of a clear plateau, although the concentration in the equilibrium was high. Consequently, it should be taken into account that the estimation is valid in the concentration range of the study, and any extrapolation outside, such as the predicted saturation capacity (q_s), must be considered with caution. The Sips model combines the Freundlich and Langmuir models, in which the parameter n_S stands for the deviation among them (Wang and Guo, 2020). The value of n_s indicates the affinity of the adsorbate to the adsorbent and the number of occupied sites by each adsorbate molecule (Cassol et al., 2014). The sample SRF-CO$_2$ was the one that provided the highest n_s value over the unit, indicating a high efficiency in the low concentration range.

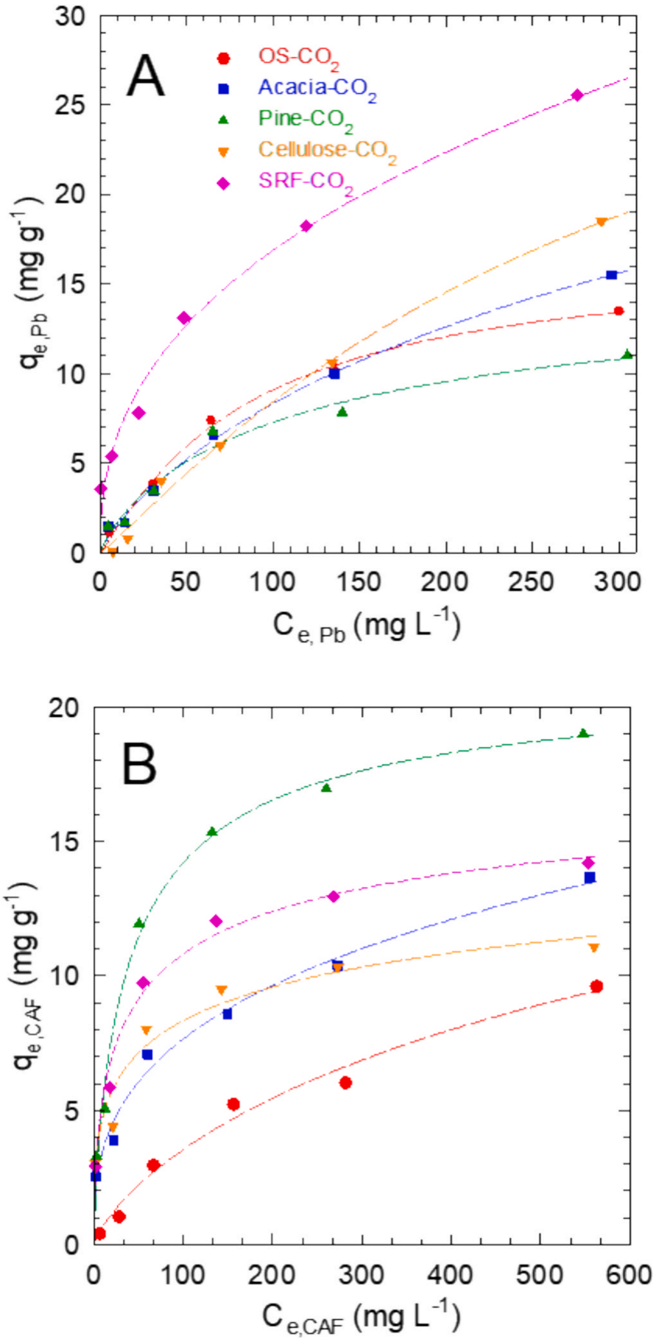

Fig. 6. Adsorption isotherms of physically activated chars for removing Pb^{2+} (A) and caffeine (B). *The dashed lines represent the fit to the Sips model. Experimental conditions:* $C_0 = 10\text{–}650$ mg L^{-1}; $C_{adsorbent} = 2$ g L^{-1}; $T = 25$ °C.

Moreover, it was the least microporous, evidence of a process not driven by microporous development. The adsorption process of metals takes place by surface covering and further diffusion of ions into the pores. The radius of hydrated Pb^{2+} is around 0.401 nm, a value very close to the dominant micropore size of the samples, whose activation built micropores of around 0.5 nm (Shahrokhi-Shahraki et al., 2021), which may compromise the diffusion of the hydrated metal to the active adsorption sites. Besides, the involved mechanism includes surface complexation, electrostatic attraction of the surface and the hydrated metal, and precipitation (Zhang et al., 2021); i.e. in the case of Pb^{2+}, it starts to precipitate as $Pb(OH)_2$ at pH over 6.0 (Liu and Liu, 2003). The enriched oxygen content and the presence of important mesoporosity of SRF-CO_2 may explain the higher Pb^{2+} uptake.

Table 3
Fitting parameters to the Sips model of the adsorption isotherms of Pb^{2+} and caffeine.

Material	q_{exp}* (mg g^{-1})	$q_e = \frac{q_S(K_S C_e)^{1/n_S}}{1 + (K_S C_e)^{1/n_S}}$			
		q_S (mg g^{-1})	K_S (L $mg^{-1})^{1/nS}$	n_S	R^2
Adsorption of Pb^{2+}					
OS-CO_2	9.6	16.75	$1.166 \cdot 10^{-2}$	0.897	0.996
Acacia-CO_2	13.7	40.03	$1.917 \cdot 10^{-3}$	1.236	0.995
Pine-CO_2	19.0	15.81	$8.269 \cdot 10^{-3}$	1.182	0.984
Cellulose-CO_2	11.1	39.45	$3.066 \cdot 10^{-3}$	0.907	0.994
SRF-CO_2	14.2	541.4	$2.820 \cdot 10^{-6}$	2.381	0.985
Adsorption of caffeine					
OS-CO_2	13.5	24.15	$9.963 \cdot 10^{-4}$	1.309	0.984
Acacia-CO_2	15.5	191.3	$1.070 \cdot 10^{-6}$	2.882	0.985
Pine-CO_2	11.0	21.56	$2.820 \cdot 10^{-6}$	1.302	0.992
Cellulose-CO_2	18.5	20.43	$3.550 \cdot 10^{-3}$	2.786	0.982
SRF-CO_2	25.5	18.87	$1.772 \cdot 10^{-2}$	1.949	0.984

* Highest experimental uptake.

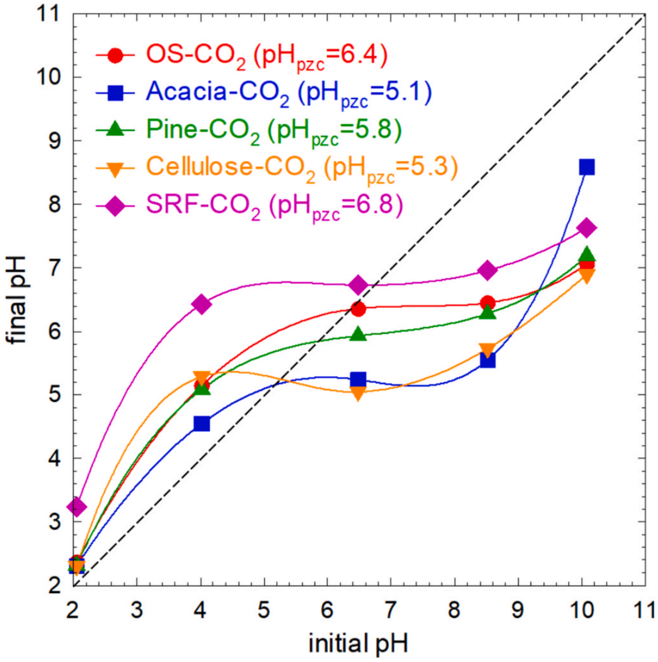

Fig. 7. Determination of the pH_{pzc} by the titration method.

The adsorption capability of caffeine with the activated samples led to the order pine-CO_2 (19.0 mg g^{-1}) > SRF-CO_2 (14.2 mg g^{-1}) ~ Acacia-CO_2 (13.7 mg g^{-1}) > Cellulose-CO_2 (11.0 mg g^{-1}) > OS-CO_2 (9.6 mg g^{-1}). In this case, the plateau uptake of the isotherm was almost defined, although the concentration at which they appeared was high, see Fig. 6B. The experimental data were successfully fitted to the three-parameter Sips model (Sips, 1948), leading to the parameters presented in Table 3. This model was selected based on the suitability for the prediction onto heterogeneous surfaces, avoiding the limitation of increased adsorbate concentration normally associated with the Freundlich model (Ayawei et al., 2017). Most of the fittings led to a Sips exponent superior to the unit, which indicates that the adsorption process is favorable at low adsorbate concentration (Cassol et al., 2014). According to the literature, caffeine adsorption is highly influenced by the pore volume (Bachmann et al., 2021; Couto et al., 2015). All the activated chars displayed a pore volume in the range of 0.192–0.225 cm^3 g^{-1}, which may explain great differences between their adsorption uptakes. These values might be labeled as low-moderate and not impressive if compared to the much higher values of astonishingly

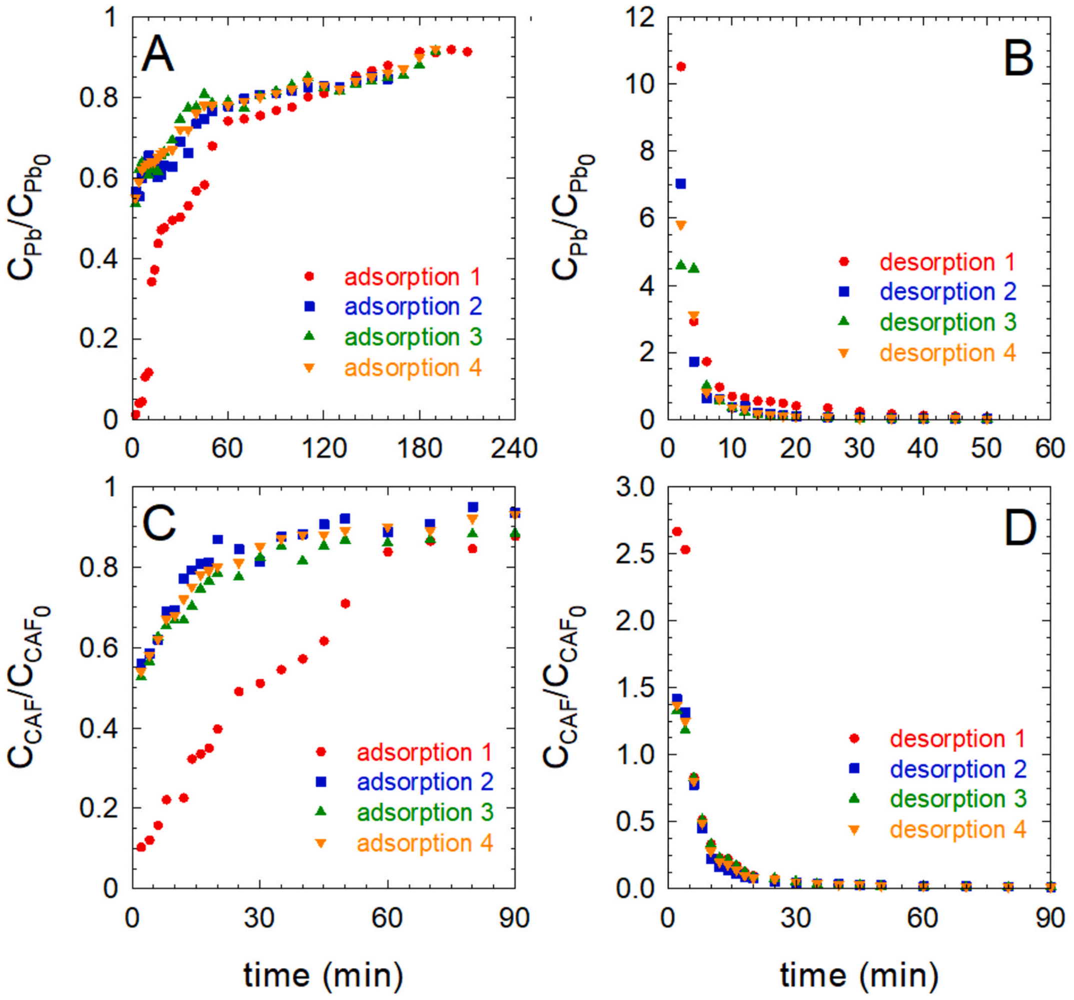

Fig. 8. Breakthrough columns of adsorption and desorption cycles of Pb onto SRF-CO_2 (A and B) and caffeine with Pine-CO_2 (C and D). Experimental conditions: C_0 = 20 mg L^{-1}; $m_{adsorbent}$ = 0.5 g; T = 25 °C, Q = 2 mL min^{-1}; desorption carried out with HCl 1 M for Pb and methanol for caffeine.

porous carbon materials (Bachmann et al., 2021), based on a more aggressive activation process, generally KOH (Pereira et al., 2024).

The plausible electrostatic interactions between the surface of the materials and the adsorbate were assessed by a combination of the $pH_{pzc,}$ which establishes the nature of the charge at the surface of the solid, and the speciation of the substance at the pH of the experiment. Fig. 7 illustrates the pH_{pzc} determination by the titration method, leaving to values within 4–6. The adsorption behavior of lead and caffeine in aqueous solution may be influenced by the pH_{pzc} as the surface is negatively charged at pH values higher than pH_{pzc} and positively charged at pH values below the pH_{pzc}. On the one hand, Pb adsorption increases at pH values above the pH_{PZC} due to electrostatic attraction between the negatively charged surface and the cationic species (Dhahri et al., 2022; Zaini et al., 2009). However, the solution pH during this experiment, although dependent on the Pb concentration, was within 5.3–5.8, values which are close to the pH_{pzc}. Therefore, other interactions of a different nature may take place, such as surface complexation (Zhang et al., 2021). On the other hand, although caffeine remains predominantly neutral across a wide pH range due to its relatively high pK_a (~10.4) (Bachmann et al., 2021), pH can still influence its adsorption behavior through several mechanisms. At low pH, adsorption may be enhanced via non-electrostatic mechanisms such as hydrogen bonding between the nitrogen atoms of the caffeine molecule and positively charged carboxyl groups on the surface, which are the main forces, as the pH of the caffeine solution was 4.2–5.8 (Bachmann et al., 2021; Melo et al., 2020).

The behavior under dynamic conditions was tested, selecting for each contaminant the adsorbent with the best performance according to the highest experimental adsorption uptake. In the case of Pb^{2+}, it was SRF-$CO_{2,}$ and in the case of caffeine, it was pine-CO_2. Fig. 8 illustrates three consecutive adsorption and desorption cycles in each case. In the case of Pb^{2+}, pictured in Fig. 8A-B, it is appreciated that the column performance losses efficiency from the first cycle to the second, as the Pb^{2+} capacity dropped from 4.67 (1st run) to 2.96 mg g^{-1} (2nd run), being almost constant in the following reusing cycles, i.e. 3.11 mg g^{-1} (3rd run) and 3.05 mg g^{-1} (4th run). This partial loss after the first cycle can be ascribed to a partial fixation of Pb^{2+} that is not subsequently released in the desorption step, blocking part of the active sites, as reported commonly in Pb^{2+} adsorption with other biochar formulas (Mahdi et al., 2018). The first desorption cycle released 3.14 mg g^{-1}, which equals 67 % of desorption efficiency, and after this cycle, the desorbed amount was roughly 90 %. Other works have reported modification of the textural properties during the regeneration with acid (Wang et al., 2015), which was not the case since the measured surface area of the SRF-CO_2 material after the 4th run was very similar to the initial one, concretely 136 vs 181 m^2 g^{-1}, before and after utilization, respectively. In the case of caffeine, similar behavior has been recorded, see Fig. 8C and D. The adsorption uptakes were 2.74 (1st run), 1.06 (2nd run), 1.33 (3rd run), and 1.23 mg g^{-1} (4th run). A considerable retention decay was registered after the first run, despite recovering over 90 % in the first desorption run. In this case, the regeneration with methanol may have affected the surface properties, leading to less effective adsorption centers. Overall, the fixed-bed column tests manifested that the material can be regenerated and used in sequential cycles, although settling in the first cycle is required after the first regeneration step.

4. Conclusions

Physical activation with CO_2 of chars recovered from pyrolysis valorization is a suitable technology for preparing porous materials; however, the porosity developed was moderate, with surface areas in the range 340–370 $m^2\ g^{-1}$ and high microporosity contribution, of over 70 % in the best chars. XPS and chemisorption characterization evidenced the presence of carbonyl and quinone groups. Therefore, the material was very efficient for the adsorption of CO_2, which interestingly enables it for a practical application of CO_2 capture and storage, such as in the post-combustion effluents, mainly ascribed to the high microporosity. However, physical activation did not perform activated carbon formulas as competitively for water treatment as those prepared under chemical activation, especially when using aggressive chemicals such as alkalis. The best Pb uptake was 25.5 mg g^{-1}, whereas the best result in caffeine removal was 17.1 mg g^{-1}. The performance in fixed-bed column assays showed that the regeneration step affects the uptake of the following cycle; however, after a first regeneration stabilization, it led to a stable behavior. Although these values may be labeled as low-moderate, depending on the nature of the polluted effluent, the physically obtained formulas may be suitable, since the concentration level at which the contaminants of emerging concern, usually in the range of ppb or lower, is still far from the saturation level uptake of the prepared adsorbents. These deterring limitations could be largely overcome by the benefits associated, such as the needless use of aggressive chemicals, like toxic alkalis, or additional washing steps for removing the chemical excess. Specific target application, e.g. gas or liquid treatment, can be tackled depending on the textural properties achieved, which are influenced by the origin of the char precursor, i.e. biomass or polymeric-based residues. Additional chemical post-treatment can aid in the modification of the surface chemistry via functionalization and, therefore, improve certain adsorbates' anchorage. Overall, physical activation methods may be a potential alternative to boost a more respectful and sustainable activation process.

CRediT authorship contribution statement

Ledicia Pereira: Visualization, Investigation, Conceptualization. **Mónica Calero:** Writing – review & editing, Project administration, Investigation, Funding acquisition, Conceptualization. **Gabriel Blázquez:** Investigation. **Sergio González-Egido:** Resources, Funding acquisition. **María González-Lucas:** Resources, Funding acquisition. **M. Ángeles Martín-Lara:** Writing – review & editing, Supervision, Investigation, Funding acquisition, Conceptualization. **Rafael R. Solís:** Writing – review & editing, Writing – original draft, Visualization, Investigation, Conceptualization.

Declaration of competing interest

The authors declare that they have no known competing financial interests or personal relationships that could have appeared to influence the work reported in this paper.

Acknowledgments

The authors acknowledge the Ministry of Science, the State Research Agency, and the European Union for the project AGROMITCAR (project CPP2021-008551 financed by MCIN/AEI/10.13039/501100011033 and the European Union Next Generation EU/PRTR). They also thank the support provided for the external investigation services of the University of Granada (*Centro de Instrumentación Científica*, CIC). Finally, the authors acknowledge *Neoliquid Advanced Biofuels and Biochemicals S.L.* for providing the industrial chars. Funding for open access charge: Universidad de Granada/CBUA.

Data availability

Data will be made available on request.

References

Tejaswini, M.S.S.R., Pathak, P., Gupta, D.K., 2022. Sustainable approach for valorization of solid wastes as a secondary resource through urban mining. J. Environ. Manage. 319, 115727. https://doi.org/10.1016/J.JENVMAN.2022.115727.

Gardiner, R., Hajek, P., 2020. Municipal waste generation, R&D intensity, and economic growth nexus – A case of EU regions. Waste Manag. 114, 124–135. https://doi.org/10.1016/J.WASMAN.2020.06.038.

Bhatt, M., Chakinala, A.G., Joshi, J.B., Sharma, A., Pant, K.K., Shah, K., Sharma, A., 2021. Valorization of solid waste using advanced thermo-chemical process: A review. J. Environ. Chem. Eng. 9, 105434. https://doi.org/10.1016/J.JECE.2021.105434.

Qureshi, M.S., Oasmaa, A., Pihkola, H., Deviatkin, I., Tenhunen, A., Mannila, J., Minkkinen, H., Pohjakallio, M., Laine-Ylijoki, J., 2020. Pyrolysis of plastic waste: Opportunities and challenges. J. Anal. Appl. Pyrol. 152, 104804. https://doi.org/10.1016/J.JAAP.2020.104804.

Apaydin-Varol, E., Pütün, A.E., 2012. Preparation and characterization of pyrolytic chars from different biomass samples. J. Anal. Appl. Pyrol. 98, 29–36. https://doi.org/10.1016/J.JAAP.2012.07.001.

Martín-Lara, M.A., Piñar, A., Ligero, A., Blázquez, G., Calero, M., 2021. Characterization and use of char produced from pyrolysis of post-consumer mixed plastic waste. Water (basel) 13, 1188. https://doi.org/10.3390/W13091188.

Z. Heidarinejad, M.H. Dehghani, M. Heidari, G. Javedan, I. Ali, M. Sillanpää, Methods for preparation and activation of activated carbon: a review, Environmental Chemistry Letters 2020 18:2 18 (2020) 393–415. https://doi.org/10.1007/S10311-019-00955-0.

Gao, Y., Yue, Q., Gao, B., Li, A., 2020. Insight into activated carbon from different kinds of chemical activating agents: A review. Sci. Total Environ. 746, 141094. https://doi.org/10.1016/J.SCITOTENV.2020.141094.

Sevilla, M., Fuertes, A.B., 2016. A Green Approach to High-Performance Supercapacitor Electrodes: The Chemical Activation of Hydrochar with Potassium Bicarbonate. ChemSusChem 9, 1880–1888. https://doi.org/10.1002/CSSC.201600426.

A.K. Sakhiya, A. Anand, P. Kaushal, Production, activation, and applications of biochar in recent times, Biochar 2020 2:3 2 (2020) 253–285. https://doi.org/10.1007/S42773-020-00047-1.

González, J.F., Román, S., González-García, C.M., Nabais, J.M.V., Ortiz, A.L., 2009. Porosity Development in Activated Carbons Prepared from Walnut Shells by Carbon Dioxide or Steam Activation. Ind. Eng. Chem. Res. 48, 7474–7481. https://doi.org/10.1021/IE801848X.

M. Javed, M. Zahoor, S.A. Mazari, S.S. Qureshi, N. Sabzoi, A.S. Jatoi, N.M. Mubarak, An overview of effect of process parameters for removal of CO_2 using biomass-derived adsorbents, Biomass Conversion and Biorefinery 2021 13:6 13 (2021) 4495–4513. https://doi.org/10.1007/S13399-021-01548-0.

Liu, W.J., Jiang, H., Yu, H.Q., 2015. Development of Biochar-Based Functional Materials: Toward a Sustainable Platform Carbon Material. Chem. Rev. 115, 12251–12285. https://doi.org/10.1021/ACS.CHEMREV.5B00195.

Thakur, A., Kumar, A., 2024. Unraveling the multifaceted mechanisms and untapped potential of activated carbon in remediation of emerging pollutants: A comprehensive review and critical appraisal of advanced techniques. Chemosphere 346, 140608. https://doi.org/10.1016/J.CHEMOSPHERE.2023.140608.

Lee, C.C., Zhao, Y.N., 2023. Heterogeneity analysis of factors influencing CO_2 emissions: The role of human capital, urbanization, and FDI. Renew. Sustain. Energy Rev. 185, 113644. https://doi.org/10.1016/J.RSER.2023.113644.

Gunawardene, O.H.P., Gunathilake, C.A., Vikrant, K., Amaraweera, S.M., 2022. Carbon Dioxide Capture through Physical and Chemical Adsorption Using Porous Carbon Materials: A Review. Atmosphere (basel) 13, 397. https://doi.org/10.3390/ATMOS13030397.

Mariana, M., Abdul, A.K., Mistar, E.M., Yahya, E.B., Alfatah, T., Danish, M., Amayreh, M., 2021. Recent advances in activated carbon modification techniques for enhanced heavy metal adsorption. J. Water Process Eng. 43, 102221. https://doi.org/10.1016/J.JWPE.2021.102221.

Jeirani, Z., Niu, C.H., Soltan, J., 2017. Adsorption of emerging pollutants on activated carbon. Rev. Chem. Eng. 33, 491–522. https://doi.org/10.1515/REVCE-2016-0027.

Rashid, R., Shafiq, I., Akhter, P., Iqbal, M.J., Hussain, M., 2021. A state-of-the-art review on wastewater treatment techniques: the effectiveness of adsorption method. Environ. Sci. Pollut. Res. 28, 9050–9066. https://doi.org/10.1007/S11356-021-12395-X.

Malini, K., Selvakumar, D., Kumar, N.S., 2023. Activated carbon from biomass: Preparation, factors improving basicity and surface properties for enhanced CO_2 capture capacity – A review. Journal of CO_2 Utilization 67, 102318. https://doi.org/10.1016/J.JCOU.2022.102318.

Pérez-Huertas, S., Calero, M., Ligero, A., Pérez, A., Terpiłowski, K., Martín-Lara, M.A., 2023. On the use of plastic precursors for preparation of activated carbons and their evaluation in CO_2 capture for biogas upgrading: a review. Waste Manag. 161, 116–141. https://doi.org/10.1016/J.WASMAN.2023.02.022.

Abuelnoor, N., AlHajaj, A., Khaleel, M., Vega, L.F., Abu-Zahra, M.R.M., 2021. Activated carbons from biomass-based sources for CO_2 capture applications. Chemosphere 282, 131111. https://doi.org/10.1016/J.CHEMOSPHERE.2021.131111.

Dombrowski, R.J., Lastoskie, C.M., Hyduke, D.R., 2001. The Horvath–Kawazoe method revisited. Colloids Surf A Physicochem Eng Asp 187–188, 23–39. https://doi.org/10.1016/S0927-7757(01)00618-5.

Gauden, P.A., Terzyk, A.P., Rychlicki, G., Kowalczyk, P., Ćwiertnia, M.S., Garbacz, J.K., 2004. Estimating the pore size distribution of activated carbons from adsorption data of different adsorbates by various methods. J. Colloid Interface Sci. 273, 39–63. https://doi.org/10.1016/J.JCIS.2003.08.033.

Rajah, Z., Guiza, M., Solís, R.R.R., Becheikh, N., Rivas, F.J.J., Ouederni, A., 2019. Clopyralid degradation using solar-photocatalytic/ozone process with olive stone activated carbon. J. Environ. Chem. Eng. 7, 102900. https://doi.org/10.1016/j.jece.2019.102900.

Pereira, L., Castillo, V., Calero, M., González-Egido, S., Martín-Lara, M.Á., Solís, R.R., 2024. Promoting the circular economy: Valorization of a residue from industrial char to activated carbon with potential environmental applications as adsorbents. J. Environ. Manage. 356, 120753. https://doi.org/10.1016/J.JENVMAN.2024.120753.

Ligero, A., Solís, R.R., Blázquez, G., Muñoz-Batista, M.J., Pérez, A., Calero, M., 2024. On the cutting-edge of non-recyclable plastic waste valorization: From pyrolysis char to nitrogen-enriched activated carbon for landfill biogas upgrading. J. Environ. Chem. Eng. 12, 112265. https://doi.org/10.1016/J.JECE.2024.112265.

He, S., Chen, G., Xiao, H., Shi, G., Ruan, C., Ma, Y., Dai, H., Yuan, B., Chen, X., Yang, X., 2021. Facile preparation of N-doped activated carbon produced from rice husk for CO_2 capture. J. Colloid Interface Sci. 582, 90–101. https://doi.org/10.1016/J.JCIS.2020.08.021.

Bell, J.G., Benham, M.J., Thomas, K.M., 2021. Adsorption of carbon dioxide, water vapor, nitrogen, and sulfur dioxide on activated carbon for capture from flue gases: Competitive adsorption and selectivity aspects. Energy Fuel 35, 8102–8116. https://doi.org/10.1021/ACS.ENERGYFUELS.1C00339.

Liao, Y., Weber, J., Faul, C.F.J., 2015. Fluorescent microporous polyimides based on perylene and triazine for highly CO_2-selective carbon materials. Macromolecules 48, 2064–2073. https://doi.org/10.1021/MA501662R.

Solís, R.R., González, M.del C., Blázquez, G., Calero, M., Martín-Lara, M.Á., 2023. Activated char from the co-pyrolysis of polystyrene and olive stone mixtures for the adsorption of CO_2. J. Environ. Chem. Eng. 11, 111370. https://doi.org/10.1016/J.JECE.2023.111370.

Sips, R., 1948. On the structure of a catalyst surface. J. Chem. Phys. 16, 490–495. https://doi.org/10.1063/1.1746922.

Lim, C., Jeong, S.G., Ha, S., Ha, N., Myeong, S., Lee, Y.S., 2023. Unique CO_2 adsorption of pine needle biochar-based activated carbons by induction of functionality transition. J. Ind. Eng. Chem. 124, 201–210. https://doi.org/10.1016/J.JIEC.2023.04.008.

Solís, R.R., Calero, M., Pereira, L., Ramírez, S., Blázquez, G., Martín-Lara, M.Á., 2024. Transforming a mixture of real post-consumer plastic waste into activated carbon for biogas upgrading. Process Saf. Environ. Prot. 190, 298–315. https://doi.org/10.1016/J.PSEP.2024.07.022.

Patel, H., Weldekidan, H., Mohanty, A., Misra, M., 2023. Effect of physicochemical activation on CO_2 adsorption of activated porous carbon derived from pine sawdust. Carbon Capture Sci. Technol. 8, 100128. https://doi.org/10.1016/J.CCST.2023.100128.

Román, S., González, J.F., González-García, C.M., Zamora, F., 2008. Control of pore development during CO_2 and steam activation of olive stones. Fuel Process. Technol. 89, 715–720. https://doi.org/10.1016/J.FUPROC.2007.12.015.

Bourafa, A., Berrich, E., Belhachemi, M., Jellali, S., Jeguirim, M., 2023. Preparation and characterization of hydrochars and CO_2-activated hydrochars from date and olive stones. Biomass Convers. Biorefin. 1–12. https://doi.org/10.1007/S13399-023-04225-6.

Danish, M., Hashim, R., Mohamad Ibrahim, M.N., Sulaiman, O., 2013. Characterization of physically activated Acacia mangium wood-based carbon for the removal of methyl orange dye. Bioresources 8 4323–4339. https://doi.org/10.15376/biores.8.3.4323-4339.

Ligero, A., Calero, M., Pérez, A., Solís, R.R., Muñoz-Batista, M.J., Martín-Lara, M.Á., 2023. Low-cost activated carbon from the pyrolysis of post-consumer plastic waste and the application in CO_2 capture. Process Saf. Environ. Prot. 173, 558–566. https://doi.org/10.1016/J.PSEP.2023.03.041.

Sing, K.S.W., Everett, D.H., Haul, R.A.W., Moscou, L., Pierotti, R.A., Rouquerol, J., Siemieniewska, T., 1985. Reporting Physisorption Data for Gas/Solid Systems with Special Reference to the Determination of Surface Area and Porosity. Pure Appl. Chem. 57, 603–619. https://doi.org/10.1351/PAC198557040603.

Serafin, J., Narkiewicz, U., Morawski, A.W., Wróbel, R.J., Michalkiewicz, B., 2017. Highly microporous activated carbons from biomass for CO_2 capture and effective micropores at different conditions. Journal of CO_2 Utilization 18, 73–79. https://doi.org/10.1016/J.JCOU.2017.01.006.

Thommes, M., Kaneko, K., Neimark, A.V., Olivier, J.P., Rodríguez-Reinoso, F., Rouquerol, J., Sing, K.S.W., 2015. Physisorption of gases, with special reference to the evaluation of surface area and pore size distribution (IUPAC Technical Report). Pure Appl. Chem. 87, 1051–1069. https://doi.org/10.1515/pac-2014-1117.

Bläker, C., Muthmann, J., Pasel, C., Bathen, D., 2019. Characterization of Activated Carbon Adsorbents – State of the Art and Novel Approaches. ChemBioEng Rev. 6, 119–138. https://doi.org/10.1002/CBEN.201900008.

Di Blasi, C., 2009. Combustion and gasification rates of lignocellulosic chars. Prog. Energy Combust. Sci. 35, 121–140. https://doi.org/10.1016/J.PECS.2008.08.001.

García Martín, J.F., Cuevas, M., Feng, C.H., Mateos, P.Á., García, M.T., Sánchez, S., 2020. Energetic Valorisation of Olive Biomass: Olive-Tree Pruning, Olive Stones and Pomaces. Processes 8 511. https://doi.org/10.3390/PR8050511.

Ramírez-Valencia, L.D., Bailón-García, E., Moral-Rodríguez, A.I., Carrasco-Marín, F., Pérez-Cadenas, A.F., 2023. Carbon Gels–Green Graphene Composites as Metal-Free Bifunctional Electro-Fenton Catalysts. Gels 9, 665. https://doi.org/10.3390/GELS9080665.

Burg, P., Fydrych, P., Cagniant, D., Nanse, G., Bimer, J., Jankowska, A., 2002. The characterization of nitrogen-enriched activated carbons by IR, XPS and LSER methods. Carbon N Y 40, 1521–1531. https://doi.org/10.1016/S0008-6223(02)00004-0.

Shafeeyan, M.S., Daud, W.M.A.W., Houshmand, A., Shamiri, A., 2010. A review on surface modification of activated carbon for carbon dioxide adsorption. J. Anal. Appl. Pyrol. 89, 143–151. https://doi.org/10.1016/J.JAAP.2010.07.006.

Rocha, R.P., Pereira, M.F.R., Figueiredo, J.L., 2023. Characterisation of the surface chemistry of carbon materials by temperature-programmed desorption: An assessment. Catal. Today 418, 114136. https://doi.org/10.1016/J.CATTOD.2023.114136.

Herold, F., Gläsel, J., Etzold, B.J.M., Rønning, M., 2022. Can Temperature-Programmed Techniques Provide the Gold Standard for Carbon Surface Characterization? Chem. Mater. 34, 8490–8516. https://doi.org/10.1021/ACS.CHEMMATER.2C02449.

Rodriguez-Reinoso, F., Molina-Sabio, M., Muñecas, M.A., 1992. Effect of microporosity and oxygen surface groups of activated carbon in the adsorption of molecules of different polarity. J. Phys. Chem. 96, 2707–2713. https://doi.org/10.1021/J100185A056.

Shen, Y., 2022. Preparation of renewable porous carbons for CO_2 capture – A review. Fuel Process. Technol. 236, 107437. https://doi.org/10.1016/J.FUPROC.2022.107437.

Mochizuki, Y., Bud, J., Byambajav, E., Tsubouchi, N., 2024. Pore properties and CO_2 adsorption performance of activated carbon prepared from various carbonaceous materials. Carbon Resour. Convers., 100237 https://doi.org/10.1016/J.CRCON.2024.100237.

He, M., Zhao, H., Yang, X., Jia, J., Liu, X., Qu, Z., Zhou, W., Sun, F., Wang, Z., 2023. Reconsideration about the competitive adsorption of H_2O and CO_2 on carbon surfaces: The influence of oxygen functional groups. J. Environ. Chem. Eng. 11, 111288. https://doi.org/10.1016/J.JECE.2023.111288.

Liu, B., Li, H., Ma, X., Chen, R., Wang, S., Li, L., 2018. The synergistic effect of oxygen-containing functional groups on CO_2 adsorption by the glucose–potassium citrate-derived activated carbon. RSC Adv. 8, 38965–38973. https://doi.org/10.1039/C8RA05523H.

Puig-Gamero, M., Esteban-Arranz, A., Sanchez-Silva, L., Sanchez, P., 2021. Obtaining activated biochar from olive stone using a bench scale high-pressure thermobalance. J. Environ. Chem. Eng. 9, 105374. https://doi.org/10.1016/J.JECE.2021.105374.

González, A.S., Plaza, M.G., Rubiera, F., Pevida, C., 2013. Sustainable biomass-based carbon adsorbents for post-combustion CO_2 capture. Chem. Eng. J. 230, 456–465. https://doi.org/10.1016/J.CEJ.2013.06.118.

Heo, Y.J., Park, S.J., 2015. A role of steam activation on CO_2 capture and separation of narrow microporous carbons produced from cellulose fibers. Energy 91, 142–150. https://doi.org/10.1016/J.ENERGY.2015.08.033.

Singh, G., Lakhi, K.S., Kim, I.Y., Kim, S., Srivastava, P., Naidu, R., Vinu, A., 2017. Highly Efficient Method for the Synthesis of Activated Mesoporous Biocarbons with Extremely High Surface Area for High-Pressure CO_2 Adsorption. ACS Appl. Mater. Interfaces 9, 29782–29793. https://doi.org/10.1021/ACSAMI.7B08797.

Alabadi, A., Razzaque, S., Yang, Y., Chen, S., Tan, B., 2015. Highly porous activated carbon materials from carbonized biomass with high CO_2 capturing capacity. Chem. Eng. J. 281, 606–612. https://doi.org/10.1016/J.CEJ.2015.06.032.

Fan, W., Chakraborty, A., Kayal, S., 2016. Adsorption cooling cycles: Insights into carbon dioxide adsorption on activated carbons. Energy 102, 491–501. https://doi.org/10.1016/J.ENERGY.2016.02.112.

Saleh, T.A., 2022. Adsorption technology and surface science. Interface Science and Technology 34, 39–64. https://doi.org/10.1016/B978-0-12-849876-7.00006-3.

Sarwar, A., Ali, M., Khoja, A.H., Nawar, A., Waqas, A., Liaquat, R., Naqvi, S.R., Asjid, M., 2021. Synthesis and characterization of biomass-derived surface-modified activated carbon for enhanced CO_2 adsorption. Journal of CO_2 Utilization 46, 101476. https://doi.org/10.1016/J.JCOU.2021.101476.

Tan, Y.L., Islam, M.A., Asif, M., Hameed, B.H., 2014. Adsorption of carbon dioxide by sodium hydroxide-modified granular coconut shell activated carbon in a fixed bed. Energy 77, 926–931. https://doi.org/10.1016/J.ENERGY.2014.09.079.

Hook, R.J., 1997. An Investigation of Some Sterically Hindered Amines as Potential Carbon Dioxide Scrubbing Compounds. Ind. Eng. Chem. Res. 36, 1779–1790. https://doi.org/10.1021/IE9605589.

Ligero, A., Calero, M., Martín-Lara, M.Á., Blázquez, G., Solís, R.R., Pérez, A., 2023. Fixed-bed CO_2 adsorption onto activated char from the pyrolysis of a non-recyclable plastic mixture from real urban residues. Journal of CO_2 Utilization 73, 102517. https://doi.org/10.1016/J.JCOU.2023.102517.

Manyà, J.J., García-Morcate, D., González, B., 2020. Adsorption Performance of Physically Activated Biochars for Postcombustion CO_2 Capture from Dry and Humid Flue Gas. Appl. Sci. 10, 376. https://doi.org/10.3390/APP10010376.

S. Madhav, A. Ahamad, A.K. Singh, J. Kushawaha, S. Chauhan, S. Sharma, P. Singh, S. Madhav, Á.A. Ahamad, Á.A.K. Singh, Á.J. Kushawaha, J.S. Chauhan, Á.S. Sharma, P. Singh, Water Pollutants: Sources and Impact on the Environment and Human Health, in: Water Pollutants Monitoring: Role of Material. Advanced Functional Materials and Sensors, Springer, Singapore, 2020: pp. 43–62. https://doi.org/10.1007/978-981-15-0671-0_4.

Buerge, I.J., Poiger, T., Müller, M.D., Buser, H.R., 2003. Caffeine, an Anthropogenic Marker for Wastewater Contamination of Surface Waters. Environ. Sci. Tech. 37, 691–700. https://doi.org/10.1021/ES020125Z.

Li, S., Wen, J., He, B., Wang, J., Hu, X., Liu, J., 2020. Occurrence of caffeine in the freshwater environment: Implications for ecopharmacovigilance. Environ. Pollut. 263, 114371. https://doi.org/10.1016/J.ENVPOL.2020.114371.

G. Korekar, A. Kumar, C. Ugale, 2019. Occurrence, fate, persistence and remediation of caffeine: a review, Environ. Sci. Pollut. Res. 27, 34715–34733. https://doi.org/10.1007/S11356-019-06998-8.

Wang, J., Guo, X., 2020. Adsorption isotherm models: Classification, physical meaning, application and solving method. Chemosphere 258, 127279. https://doi.org/10.1016/J.CHEMOSPHERE.2020.127279.

Cassol, G., Gallon, R., Schwaab, M., Barbosa-Coutinho, E., Júnior, J., Pinto, J., 2014. Statistical evaluation of non-linear parameter estimation procedures for adsorption equilibrium models. Adsorpt. Sci. Technol. 32, 257–274. https://doi.org/10.1260/0263-6174.32.4.257.

Shahrokhi-Shahraki, R., Benally, C., El-Din, M.G., Park, J., 2021. High efficiency removal of heavy metals using tire-derived activated carbon vs commercial activated carbon: Insights into the adsorption mechanisms. Chemosphere 264, 128455. https://doi.org/10.1016/J.CHEMOSPHERE.2020.128455.

Zhang, Z., Wang, T., Zhang, H., Liu, Y., Xing, B., 2021. Adsorption of Pb(II) and Cd(II) by magnetic activated carbon and its mechanism. Scienceof the Total Environment 757, 143910. https://doi.org/10.1016/J.SCITOTENV.2020.143910.

Liu, Q., Liu, Y., 2003. Distribution of Pb(II) species in aqueous solutions. J. Colloid Interface Sci. 268, 266–269. https://doi.org/10.1016/S0021-9797(03)00638-6.

Ayawei, N., Ebelegi, A.N., Wankasi, D., 2017. Modelling and Interpretation of Adsorption Isotherms. J. Chem. 2017, 3039817. https://doi.org/10.1155/2017/3039817.

Bachmann, S.A.L., Calvete, T., Féris, L.A., 2021. Caffeine removal from aqueous media by adsorption: An overview of adsorbents evolution and the kinetic, equilibrium and thermodynamic studies. Science of the Total Environment 767, 144229. https://doi.org/10.1016/J.SCITOTENV.2020.144229.

Couto, O.M., Matos, I., da Fonseca, I.M., Arroyo, P.A., da Silva, E.A., de Barros, M.A.S.D., 2015. Effect of solution pH and influence of water hardness on caffeine adsorption onto activated carbons. Can. J. Chem. Eng. 93, 68–77. https://doi.org/10.1002/CJCE.22104.

Dhahri, R., Yılmaz, M., Mechi, L., Alsukaibi, A.K.D., Alimi, F., Ben Salem, R., Moussaoui, Y., 2022. Optimization of the Preparation of Activated Carbon from Prickly Pear Seed Cake for the Removal of Lead and Cadmium Ions from Aqueous Solution. Sustainability 14, 3245. https://doi.org/10.3390/SU14063245.

Zaini, M.A.A., Okayama, R., Machida, M., 2009. Adsorption of aqueous metal ions on cattle-manure-compost based activated carbons. J. Hazard. Mater. 170, 1119–1124. https://doi.org/10.1016/J.JHAZMAT.2009.05.090.

Melo, L.L.A., Ide, A.H., Duarte, J.L.S., Zanta, C.L.P.S., Oliveira, L.M.T.M., Pimentel, W.R.O., Meili, L., 2020. Caffeine removal using Elaeis guineensis activated carbon: adsorption and RSM studies. Environ. Sci. Pollut. Res. 27, 27048–27060. https://doi.org/10.1007/S11356-020-09053-Z.

Mahdi, Z., Yu, Q.J., El Hanandeh, A., 2018. Removal of lead(II) from aqueous solution using date seed-derived biochar: batch and column studies. Appl Water Sci 8, 1–13. https://doi.org/10.1007/S13201-018-0829-0.

Wang, S.Y., Tang, Y.K., Chen, C., Wu, J.T., Huang, Z., Mo, Y.Y., Zhang, K.X., Chen, J.B., 2015. Regeneration of magnetic biochar derived from eucalyptus leaf residue for lead(II) removal. Bioresour. Technol. 186, 360–364. https://doi.org/10.1016/J.BIORTECH.2015.03.139.